Materials Science Forum
ISSN: 1662-9752, Vol. 1183, pp 1-11
doi:10.4028/p-veE4uC

Submitted: 2026-01-19
Revised: 2026-02-17
Accepted: 2026-02-24
Online: 2026-04-13

Tailored Temperature Gradients in Hybrid Components: Influence of Variable Process Parameters under Cold and Preheated Conditions

Gerke Niklas[1,a*], Amend Hendrik[1,b], Peddinghaus Julius[1,c], Brunotte Kai[1,d] and Behrens Bernd-Arno[1,e]

[1]Leibniz University Hannover, Institute of Forming Technology and Forming Machines, An der Universität 2, 30823 Garbsen, Germany

[a*]gerke@ifum.uni-hannover.de, [b]hendrik.amend@stud.uni-hannover.de, [c]peddinghaus@ifum.uni-hannover.de, [d]brunotte@ifum.uni-hannover.de, [e]behrens@ifum.uni-hannover.de

Keywords: tailored forming, thermal management (process control), hybrid components, spray cooling, induction heating, multi-stage forming.

Abstract. Adaptive thermal management is a prerequisite for multi-stage tailored forming of hybrid steel-aluminium blocks, as each section of material must remain within its forming temperature window and the joining zone must be protected from excessive thermal stress. This study defines a control-oriented process space for a combined induction heating and dual-fluid spray cooling concept developed in the Collaborative Research Center (SFB) 1153 "Tailored Forming." A three-phase test program is applied: Phase A quantifies and evaluates the influence of air pressure p_{air}, water pressure p_w, and nozzle distance d on the cooling performance and the formation of an axial gradient using standardized regression coefficients. In phases B and C, a reference setting is applied to rotationally friction-welded 20MnCr5/EN AW-6082 blocks in a cold-start and preheated state, which are representative of multi-stage forming processes. The results show that p_{air} and p_w dominate both the cooling capacity and the formation of gradients, while d plays a subordinate role in the range investigated. The relationships remain qualitatively consistent for hybrid blanks and preheated conditions when the heating program is adapted to the aluminium and joining zone boundaries. The derived actuator ranking forms the basis for closed-loop temperature control in volatile, multi-stage tailored forming chains.

Introduction

The increasing demand for lightweight, high-performance components is driving interest in hybrid material systems that combine complementary properties within a single bulk part. In the Tailored Forming approach, a joined hybrid semi-finished workpiece is locally thermally conditioned prior to forming so that each material region reaches a material-specific forming temperature window, enabling function-integrated, weight-optimized components to be manufactured. [1, 2]

Moving from single-step studies to multi-stage Tailored Forming chains narrows permissible thermal windows and increases volatility (e.g., varying transfer times and residual heat). Therefore, temperature profiles must be not only achievable but also controllable and reproducible. Defining a control-oriented process space and reliable actuators for process-integrated thermal management is a prerequisite for robust multi-stage chains. [3]

The Collaborative Research Centre (CRC) 1153 "Tailored Forming" process chain starts from joined, semi-finished billets and combines induction heating with localized two-fluid spray cooling to establish axial gradients, followed by transfer/handling and forming steps. Because induction power and spray cooling have their own parameter space, the overall system should be well suited for adaptive control. [1, 3, 4, 5, 6]

CRC 1153 studies by Piwek et al. [3, 4, 5, 6] and Ince et al. [7] have demonstrated the feasibility and potential of tailored temperature gradients for hybrid steel–aluminium billets and linked thermal histories to joint properties and process outcomes. However, these works typically employed one selected spray setting. Thus, a transferable, control-oriented characterization of the spray parameter space-needed for multi-stage operation with higher volatility-remains missing. [3, 4, 5, 6, 7]

In this paper, the focus is on a control-oriented process-space definition for induction–spray thermal management as an enabling step for subsequent forging-stage validation within the CRC 1153 process chain. The goal is to create a high temperature gradient in order to keep the steel area as hot as possible within its forming window, thereby improving formability and reducing the yield stress discrepancy with aluminium. At the same time, the aluminium segment and the joining-zone set hard upper limits, making thermal management a selective, spatially resolved control problem rather than a global cooling task. For steel–aluminium hybrids, thermal management is particularly critical. Mismatched allowable temperatures can cause inhomogeneous softening and unstable forming conditions [8], while the joining-zone must be protected against excessive thermal exposure and brittle Fe–Al intermetallic growth [9]. In addition, the aluminium segment must stay safely below incipient melting, making allowable aluminium temperatures and exposure times hard constraints for any adaptive strategy.

Induction heating offers production-relevant cycle times and adjustable penetration depth [10, 11], but in hybrid geometries contrasts in electromagnetic and thermal properties can distort power deposition near the material transition and limit the reproducibility of heating-only gradient generation [7]. In this study, the induction setup and frequency are kept constant (penetration depth is not actively tuned). Therefore, surface heat extraction via spray cooling (air/water pressure and nozzle distance) is treated as the main adjustable actuator.

Localized two-fluid spray cooling provides flexible, tunable heat extraction to increase and maintain gradients after heating. Depending on surface temperature and heat-flux density, regimes range from single-phase convection to nucleate/transition boiling and high-temperature regimes with reduced effective heat transfer [12, 13]. In air–water systems, pressure levels shape droplet size, momentum and mass flow [14], while nozzle distance affects jet spreading and impingement distribution and thus local heat-flux density [15]. Spray cooling does not eliminate heat conduction, but counteracts heat conduction-driven homogenization by selectively removing heat where high temperatures are undesired, enabling higher and more reproducible gradients over process-relevant cycle times.

Despite this qualitative understanding, evidence remains limited on how adjustable spray parameters, together with application-oriented induction profiles, affect cooling power and axial gradients—especially under transfer conditions with different initial thermal states [16]. Systematic monomaterial reference studies and explicit transferability assessments to hybrid billets are rare, and sensitivity measures that prioritize dominant control variables for robust design and subsequent control are insufficiently reported for combined induction-heating/spray-cooling strategies [17].

The goal of this paper is to define a process space for adaptive thermal management in multi-stage Tailored Forming process chains. Phase A screens and ranks relevant adjustable spray parameters as potential control variables. Phases B and C then assess transferability across billet type and multi-stage thermal history (preheated transfer states), which is essential for process-chain implementation. This control-oriented process-space definition is intended to enable subsequent correlation with joining-zone geometry, intermetallic evolution and bond properties, as demonstrated in earlier Tailored Forming studies on steel–aluminium hybrids. [3, 4, 5, 6]

Accordingly, the research questions are structured along phases A–C to ensure a direct link between variable screening, transferability and process-chain relevance.

From this analysis, three research questions arise. First, which spray parameters (air pressure, water pressure and nozzle distance) dominate cooling power and the resulting axial temperature gradient under non-preheated initial conditions. Second, how does a preheated initial state affect the achievable gradients and the incremental cooling effect of the parameters in a multi-stage cycle. Third, can the experimental data be used to derive a robust, interpretable ranking of control variables for process design, enabling key variables to be prioritized for subsequent process control?

Materials and Methods

A three-stage experimental concept was used to identify and validate control-relevant spray-cooling actuators for process-integrated thermal management. Phase A employs monomaterial 20MnCr5 reference specimens to quantify the isolated influence of air pressure (p_{air}), water pressure (p_w) and nozzle distance (d) on cooling power and axial temperature gradients. Phase B applies the Phase-A insights to rotary-friction-welded 20MnCr5/EN AW-6082 hybrid billets starting from ambient temperature to assess transferability and the additional heat-sink effect of the aluminium segment. Phase C reproduces preheated transfer conditions of a multi-stage process chain using residual heat from a preceding heating–transfer–cooling cycle. Therefore, the induction profile is adapted to keep the aluminium segment within its allowable window and to limit joining-zone thermal exposure. Intermetallic layer growth in the Al–steel joining zone becomes critical once joining-region temperatures exceed roughly >350 °C (FeAl) and >500 °C (Fe_2Al_5-type), therefore the process window is defined to keep Tc2/Tc3 below these thresholds during cycling. [18]
All tests were conducted on cylindrical specimens (Ø 40 mm × 126 mm). Monomaterial reference specimens were manufactured from the case-hardening steel 20MnCr5 (1.7147). After rotary-friction-welding of the hybrid billets, the flash formed during the upset stage was removed using an integrated turning unit. In the hybrid sample, the length of the steel part was 100 mm and that of the aluminium part is 26 mm.

Experiments were performed on a dedicated test bench combining induction heating and active two-fluid (air–water) spray cooling. The monomaterial Phase-A design enables an interpretable actuator–response mapping without confounding effects from the dissimilar material pair, while Phases B/C evaluate qualitative transferability to hybrid billets and to preheated transfer states.

The specimen was positioned concentrically in a water-cooled copper coil which was flush with the upper edge of the sample and fixed at the top of the sample by a spring clamping system. The clamping device was insulated by a ceramic spacer. No insulation was provided at the lower mount. Induction power was applied according to defined time–power profiles, followed by a transfer/handling segment (no heating, no spray cooling) and a subsequent spray-cooling segment. Induction heating was activated at t = 0–60 s (phases A/B) and at t = 175–210 s (phase C), while spray cooling was activated in parallel. A medium-frequency generator (TruHeat MF 3010 G3 from TRUMPF Hüttinger) was operated in constant-power mode. For the main experiments, a baseline heating program of 11.3 kW for 60 s was applied. To benchmark energy-equivalent settings and identify process limits, additional power–time pairs were used (9.3 kW/80 s, 10 kW/70 s, 12.5 kW/53 s), where 12.5 kW/53 s was classified as near-critical due to incipient surface melting. For hybrid billets, the induction power was kept constant (11.3 kW) while the first heating phase was shortened to 60 s (65 s caused local melting). For multi-stage process simulation, the billet was reheated after cooling in air to 650 °C at Tc1, and a transfer time of 15 s was considered between stages. The coil geometry (turns: 6, inner diameter:52 mm, high: 40 mm) and positioning were kept constant for all tests to ensure repeatable coupling.

The vertical offset between the nozzle plane and the induction-coil mid-plane was kept constant for all experiments to decouple geometric alignment effects from the investigated spray parameters. A splash guard was installed below the coil to shield rising spray mist and minimise negative effects on heating. The schematic of the experimental setup can be seen in Fig. 1.

The nozzle spacing d was examined at discrete levels (Tab. 1) in order to compare the spacing-related changes in impact and wetting.

Four two-fluid nozzles (Type: Z-R4) were arranged around the sample body, each offset by 90 °. These nozzles are round jet air nozzles with an internal mixing pressure principle and an outlet angle of 20 °. Air and water pressures control droplet momentum, mass flow and atomisation quality, while nozzle distance controls the local impingement distribution.

The spray parameter range investigated and the reference setting used for the transfer tests are summarized in Tab. 1.

The parameter bounds were derived from preliminary trials [18] as stable operating limits of the spray system (no flooding/pulsation) while still producing clearly distinguishable cooling responses.

Although two-fluid nozzles allow wider nominal operating ranges, the investigated window was restricted by application-specific constraints (coil proximity, splash shielding to avoid mist-induced disturbances of inductive coupling, and hybrid thermal limits). In addition, a significant increase in pressure meant that temperatures above 1000°C could not be achieved. To compensate for this, the heating power was increased, which led to melting of the sample. Cooling power was evaluated over a fixed 90 s interval to ensure direct comparability between settings.

Table 1. Investigated spray-parameter space and reference setting.

Item	Symbol	Levels / range	Unit	Used in
Air pressure	p_{air}	0.6 to 1.4	bar	Phase A
Water pressure	p_w	0.2 to 0.7	bar	Phase A
Nozzle distance	d	20 / 40 / 60 / 80	mm	Phase A
Cooling-power window	Δ t	90	s	Phase A
Repetitions per setting	n	3	-	Phase A
Reference setting	-	p_{air} = 1.2, p_w = 0.6, d = 60	bar, bar, mm	Phases B and C

The thermal response was measured using four thermocouples (Tc1 to Tc4) positioned along the specimen axis. Thermocouples Tc1 to Tc3 are type K elements. The thermocouples Tc2 and Tc3 were attached by spot welding 5 mm above and below the joining zone. Tc1 and Tc4 (type J) were positioned on the end faces by spring force. The measurement positions can be found in Fig. 1. Induction heating can generate radial temperature gradients because the induced power density is concentrated near the surface (skin effect), while the bulk temperature equalizes only by heat conduction. In this work, the thermal state is therefore evaluated primarily along the surface using Tc1 to Tc4 (Fig. 1) rather than assuming a uniform cross-sectional temperature. During the spray segment, heat extraction is predominantly surface-effective, which can reduce internal gradients over time. This effect is considered when interpreting gradient evolution and phase transferability. The axial gradient indicator is defined as $\Delta T(Tc1–Tc4)$, i.e., the temperature difference between the top and bottom positions at identical time stamps of the cycle. This definition is used consistently to compare gradient magnitudes across phases and boundary conditions.

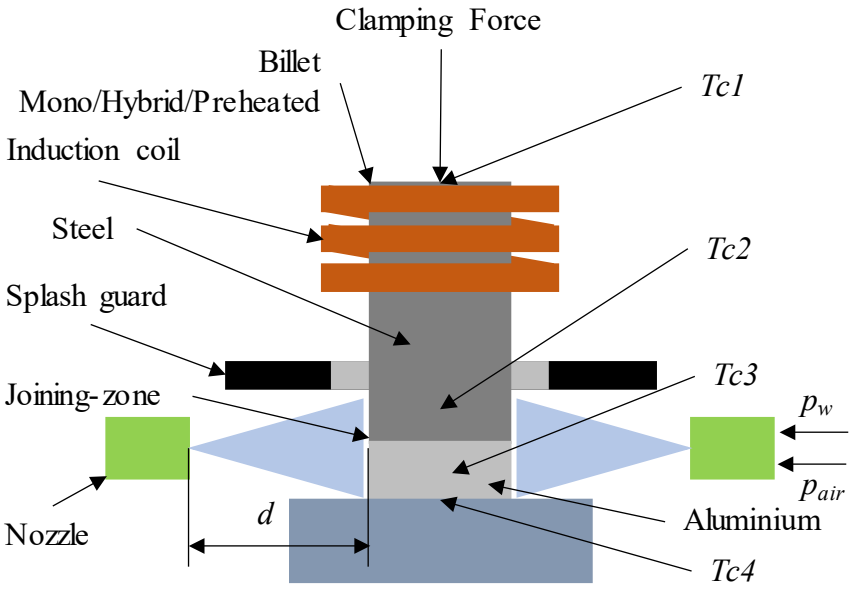

Fig. 1. Schematic of the experimental setup for induction heating and air-water spray cooling with thermocouple positions Tc1 to Tc4 and nozzle distance d.

Cooling power was quantified using a weighted temperature indicator $\bar{T}$ that represents the specimen's global thermal state while emphasizing the hotter end. Following Amend [18], $\bar{T}$ is defined as a weighted mean of Tc1 to Tc4, and the extracted heat ΔQ (Eq. 2) is calculated from the change of $\bar{T}$ over a fixed evaluation interval Δt using the specimen mass and a temperature-dependent heat capacity. The temperature-dependent specific heat capacity $c_p(T)$ used in Eq. 2 is given in Tab. 2. The values between the tabulated nodes were determined by linear interpolation. The effective cooling power is then obtained as Pcool = ΔQ/Δt (Eq. 3). This metric is used as an effective, comparative energy-balance indicator derived from the thermocouple signals for screening parameter effects and ranking actuators [10]. It is not interpreted as a strict lumped-capacitance model (Biot-number requirement) nor as a direct wall heat-flux measurement.

$$\bar{T} = (2 * Tc1 + Tc2 + Tc3 + Tc4)/5 \quad (1)$$

$$\Delta Q = m \int_{\bar{T}(t0+\Delta t)}^{\bar{T}(t1)} c_p(T)\, dT \quad (2)$$

$$Pcool = \Delta Q/t \quad (3)$$

Table 2. Temperature-dependent specific heat capacity $c_p(T)$ used in the energy-balance evaluation.

T (°C)	c_p, 20MnCr5 (J/(kg K))	c_p, EN AW-6082 (J/(kg K))
20	439.8	911.2
100	487.6	944.0
200	529.8	985.0
300	564.7	1026.0
400	605.9	1067.0
500	666.5	1108.0
600	760.2	n/a
700	1008.2	n/a
800	803.3	n/a
900	650.0	n/a
1000	650.0	n/a
1100	650.0	n/a

Here, Tc1–Tc4 denote the thermocouple temperatures, ΔQ is the extracted heat and t is the evaluation time. The weighting factor of 2 for Tc1 was taken from Amend [18] in order to increase the contribution of the hotter end of the sample in the indicator and thus improve sensitivity to gradient-related changes (Eq. 1).

To assess the combined influence of the spray parameters, data from the structured parameter study were evaluated using multiple linear regression with air pressure, water pressure and nozzle distance as predictors and cooling power as the response. Standardized regression coefficients (SRCs), obtained from z-standardized inputs, were used as the effect measure to rank the dominant actuators [19]. Each parameter setting was repeated three times (n = 3) under identical conditions. The time-resolved temperature signals were averaged at each time step.

For Phase C, preheated transfer conditions were reproduced by a multi-stage test-bench cycle rather than separate furnace preheating. After an initial heating–transfer–cooling step, the specimen was not cooled to room temperature but reheated after a defined intermediate period, yielding a preheated initial state representative of residual heat from a preceding stage (approximately Tc2 ≈ 360 °C, Tc3 ≈ 312 °C and Tc4 ≈ 130 °C at t = 175 s in the cycle: see Fig. 4). The same induction power profile was used for Phases A and B to compare monomaterial and hybrid effects under identical heating boundary conditions. In Phase C, power level and/or heating time were adjusted because the elevated initial level would otherwise overheat the aluminium segment and increase joining-zone exposure.

Results and Discussion

Phase A quantifies the isolated effects of the adjustable spray parameters (air pressure, water pressure and nozzle distance d) on cooling power and axial temperature gradients and provides a factor ranking. Phase B transfers the Phase-A setting to hybrid 20MnCr5/EN AW-6082 billets under cold-start conditions, and Phase C evaluates the influence of multi-stage thermal history by reproducing preheated transfer states.

Phase A (monomaterial 20MnCr5)

Increasing the air pressure increases cooling power markedly from 720.8 W at 0.6 bar to 973.5 W at 1.2 bar and 1475.5 W at 1.4 bar (Fig. 2a) consistent with stronger atomisation and higher droplet momentum in two-fluid sprays. Although 1.4 bar yielded a higher calculated Pcool in the screening, this setting showed insufficient reproducibility in the underlying preliminary study, and was therefore not used as the reference operating point. In Amend [18], 1.2 bar is reported as the highest reproducible cooling power within the investigated range, while the 1.4 bar value was deemed not robust due to measurement deviations. In addition to the mean trend, the data indicate increasing scatter at the upper air-pressure range, which is plausible given the transition between spray states and the sensitivity of multi-droplet impingement to local wetting dynamics. [20]

For water pressure, cooling power increases from 780.3 W (0.2 bar) to a maximum of 1030.7 W (0.6 bar) and then decreases at 0.7 bar (954.3 W), indicating a non-monotonic response within the investigated operating window (Fig. 2b). The decrease in cooling capacity at p_w = 0.7 bar despite increased liquid supply is consistent with a change in state in two-fluid spray cooling. At higher water pressure, the air-liquid ratio decreases, the droplet size may increase, and local flooding or a thicker liquid film may occur. This can reduce effective heat transfer, for example by shifting the surface towards stable film boiling conditions or by reducing atomisation quality and impact efficiency. Such non-monotonic trends with increasing liquid flow are reported for spray cooling at high surface temperatures and during quenching. [12, 13, 15, 20, 21]

For nozzle distance, the maximum occurs at d = 60 mm (780.3 W), whereas at 20 mm (721.2 W) and 80 mm (712.7 W) lower values are observed (Fig. 2c), consistent with distance-driven changes in jet spreading, droplet deceleration and impingement distribution. [15]

Based on Phase A, a robust reference setting for the subsequent transfer checks is defined as air pressure 1.2 bar, water pressure 0.6 bar and nozzle distance d = 60 mm. This setting lies within the stable operating region and yields high cooling power without relying on extreme parameter limits, which is beneficial for reproducibility and later closed-loop implementation.

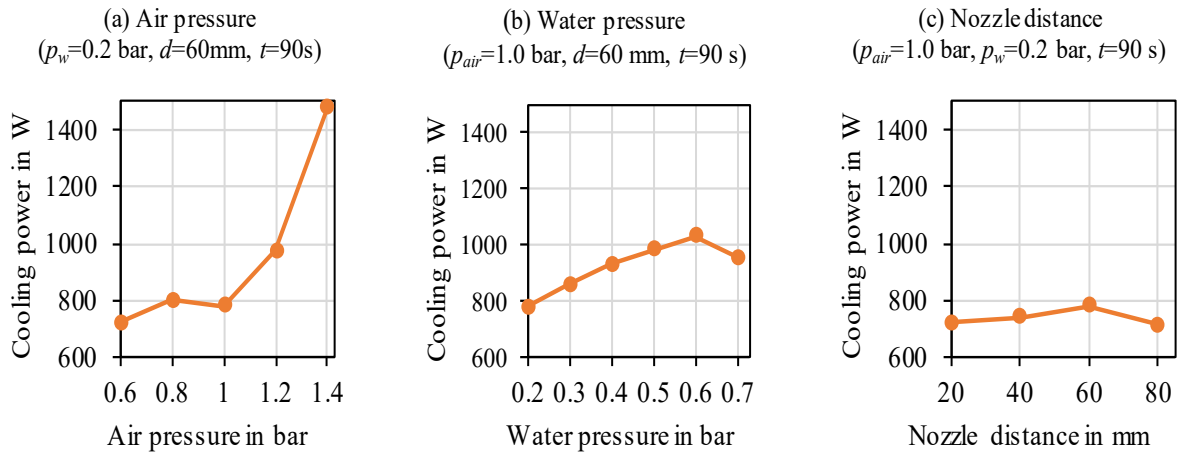

Fig. 2. Cooling power after 90 s as a function of (a) air pressure, (b) water pressure and (c) nozzle distance.

Regression-based sensitivity assessment (Fig. 3)

To quantify factor effects beyond the local trends in Fig. 2, a linear main-effects multiple linear regression (MLR) model was fitted using air pressure, water pressure and nozzle distance as predictors and cooling power as the response. Standardized regression coefficients (SRCs), obtained from z-standardized inputs, were used as a screening measure to rank the dominant, controllable actuators. [19] The SRC ranking confirms that the spray pressures are the primary control variables, while nozzle distance is secondary within the investigated range.

For robust process-chain operation, the most effective lever is the reproducible control of air and water pressure (and thus droplet momentum and mass flow), whereas nozzle distance mainly acts as a geometric tuning parameter that should be kept constant once aligned.

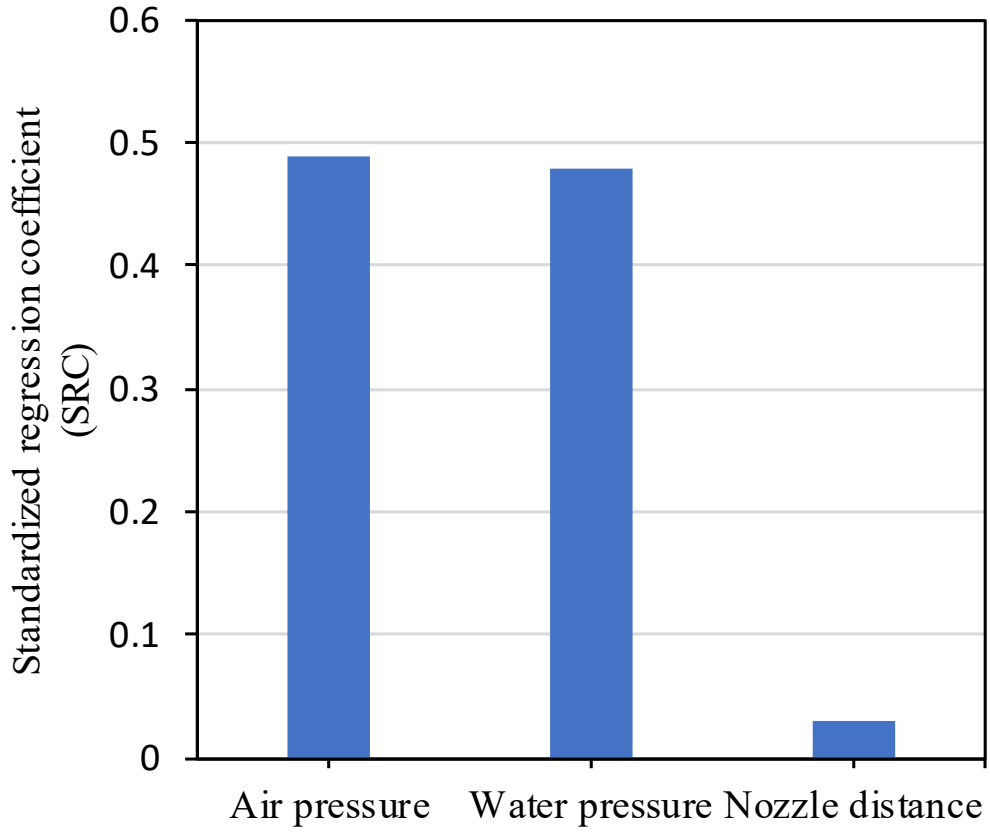

Fig. 3. Global parameter sensitivities quantified by standardized regression coefficients (SRC).

Phase B (hybrid, cold-start initial state)

Fig. 4 combines the cold-start cycle (phase B) and the subsequent reheating cycle (phase C) on a timeline. Phase B refers to the first heating and subsequent cooling segment starting from room temperature. It is important to note that the temperatures do not return to room temperature within the time window shown; the term “cooling to ambient conditions” is therefore not applicable. The second heating segment from t = 175 s belongs to phase C and represents the reheating from a preheating state generated by residual heat (see Materials and Methods).

Under identical heating and cooling conditions, the hybrid sample systematically reaches lower temperatures than the reference sample made of a single material. This is consistent with the assumption that the aluminium segment acts as an additional cooling path and changes the effective heat flow distribution. The resulting temperature values at the most important points in time (end of heating at t = 60 s and maximum temperature after heating at t = 75 s) are summarized in Tab. 3, and the complete temperature curves are shown in Fig. 4.

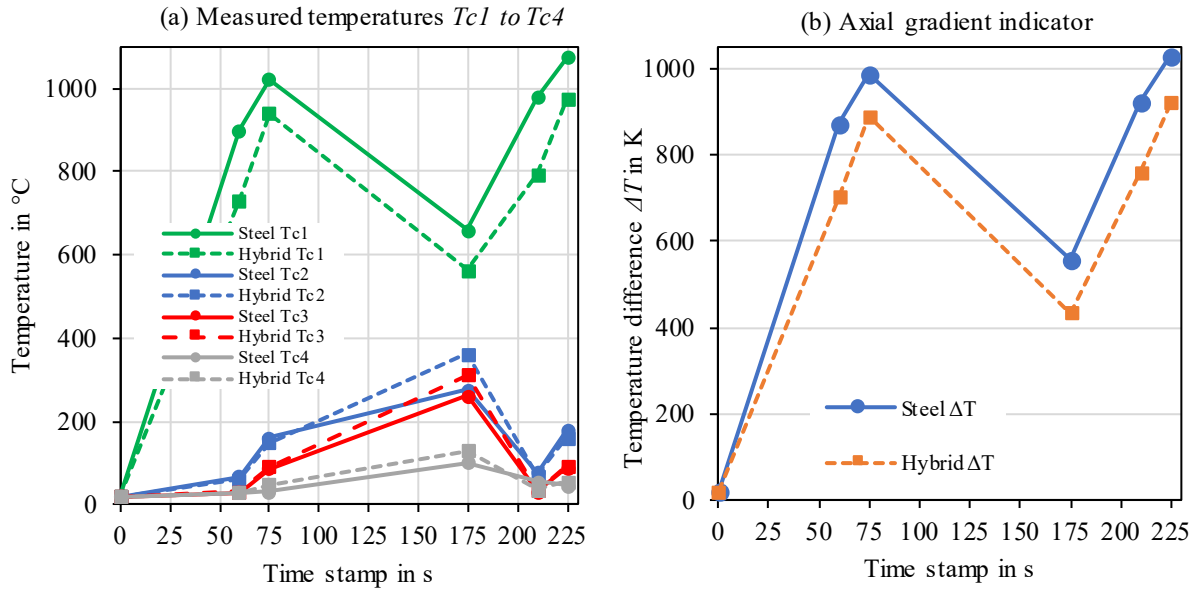

Fig. 4. a) measured temperatures (Tc1 to Tc4), b) the axial gradient indicator ΔT(Tc1−Tc4) for monomaterial 20MnCr5 and hybrid 20MnCr5/EN AW-6082.

For easier comparison, Tab. 3 summarizes the thermocouple temperatures and the axial gradient indicator at the key points in time used in Fig. 4.

Table 3. Key data points from the initial heating phase and subsequent response (Fig. 4).

t in s	Tc1 mono in °C	Tc2 mono in °C	Tc3 mono in °C	Tc4 mono in °C	ΔT mono in °C	Tc1 hyb in °C	Tc2 hyb in °C	Tc3 hyb in °C	Tc4 hyb in °C	ΔT hyb in °C
0	20	20	20	20	0	20	20	20	20	0
60	900.3	66.7	28.7	28.5	871.8	731.7	61.2	31.6	28.8	702.9
75	1021.5	160.4	85.7	32.1	989.4	939.5	148.5	90.3	49.2	890.3
175	658.4	275.1	260.7	100.7	557.7	562.7	362	311.9	129.6	433.1
210	977.9	78.2	32.5	55.1	922.8	794.6	69.7	32.9	35.5	759.1
225	1074.9	179.5	87.9	45.1	1029.8	975.5	160.1	94.8	55.7	919.8

Comparison Phase A vs. B (qualitative transferability)

The dominant control variables identified in Phase A (air and water pressure) remain effective for shaping the thermal trajectory of the hybrid billet. The absolute temperature levels and gradient magnitudes shift because the aluminium segment introduces an additional heat-sink pathway and changes the boundary conditions. Consequently, adaptive process strategies must combine spray control with appropriate heating control (e.g., power/time adaptation) for hybrid process-chain states. [1,2]

Phase C (hybrid, preheated initial state, Fig. 4)

The preheated state is generated by a reproduced multi-stage cycle (see Materials and methods). After an initial heating–transfer–cooling step, the billet is not cooled to room temperature but subsequently reheated after a defined intermediate period, yielding elevated initial temperatures representative of residual heat from a preceding stage. Compared with the cold-start case, the preheated cycle reaches comparable or moderately higher peaks after subsequent reheating, while the

inner measurement locations start from elevated levels. Therefore, heating parameters were adapted to avoid overheating the aluminium segment and to limit joining-zone thermal exposure.

During reheating in phase C (from t = 175 s), the initial temperatures are elevated due to residual heat from the previous cycle. The corresponding preheated initial state at t = 175 s is listed in Tab. 3, and the subsequent trajectories are shown in Fig. 4. These values define the deviation of the thermal history from phase B and explain the upward shift in the subsequent temperature curves. The heating parameters are therefore adjusted to prevent overheating of the aluminium segment and to limit the exposure time of the joining zone.

Comparison Phase B vs. C (thermal-history transferability)

For a better overview, Tab. 4 compares Phase B and Phase C at key points in time in Fig. 4 using directly readable values. Comparing the hybrid states at the end of the heating step (t = 60 s vs. t = 210 s) and at the at the end of the transfer segment (corresponding to the maximum temperature after heating, immediately before spray cooling) (t = 75 s vs. t = 225 s) shows qualitatively similar trajectories, with an upward shift due to the preheated initial condition. For example, Tc1 increases from 731 °C → 794 °C and 939 °C → 975 °C (Fig. 4), while Tc4 increases from 28 °C → 35 °C and 49 °C → 55 °C. These results support the conclusion that the identified control relationships remain qualitatively consistent across multi-stage initial states, provided that the allowable aluminium temperature window and the joining-zone exposure time are deliberately limited. [8,22]

Table 4. Phase B vs. Phase C comparison for the hybrid billet at the end of heating and cooling segments.

	Phase B	Tc1_B (°C)	Tc4_B (°C)	ΔT_B (°C)	Phase C	Tc1_C (°C)	Tc4_C (°C)	ΔT_C (°C)
End Heating	60 s	731	28	703	210 s	794	35	759
End Cooling	75 s	939	49	890	225 s	975	55	920

Summary and Outlook

This contribution targets the definition of a process space for adaptive thermal management in multi-stage Tailored Forming process chains. A combined strategy of induction heating and localized air–water two-fluid spray cooling is investigated to generate and maintain axial temperature gradients under process-relevant constraints (aluminium temperature window and joining-zone exposure) and under varying initial states representative of multi-stage routes. [3, 4, 5, 6] The phase-based evaluation provides a consistent storyline. In Phase A, air pressure and water pressure are identified as the dominant, controllable actuators for cooling power and gradient shaping, while nozzle distance is secondary within the investigated range. Fig. 2 and 3 jointly provide the trend-based interpretation and the global actuator ranking (SRC screening). In Phase B and Phase C, the qualitative relationships remain valid for hybrid billets and for preheated transfer states (Fig. 4), supporting transferability to multi-stage process-chain operation. Relative to prior CRC 1153 demonstrations that employed one selected spray setting, the present work contributes a control-oriented characterization and prioritization of the available spray actuators. That is an essential step toward making induction–spray thermal management regulatable in volatile multi-stage environments. Phases B/C are intentionally transfer checks (single reference setting) rather than additional full process-window explorations. Quantitative prediction across the entire hybrid parameter space therefore requires further calibration. From an implementation perspective, adaptive control should prioritize reproducible regulation of air and water pressure (fast, high leverage) and treat nozzle distance as an aligned setup parameter. The observed non-monotonic response at high water pressure also indicates that purely linear models are suitable for screening, while more detailed nonlinear mappings may be beneficial for predictive control in an extended parameter space.

Future work should expand the parameter space on hybrid billets, include systematic variations of transfer time and residual heat, and validate the identified process window in real multi-stage forming sequences. In addition, thermal states should be linked to forming-relevant quality metrics (e.g., flow behavior, bond strength and intermetallic-layer evolution) to connect thermal control to component performance. Finally, the actuator ranking and transferability evidence provided here can be used to design closed-loop temperature profiling strategies (e.g., using pyrometric feedback and pressure control) for CRC 1153-style multi-stage Tailored Forming routes, where maintaining the aluminium window and limiting joining-zone exposure are decisive constraints.

Acknowledgement

The authors thank the German Research Foundation (DFG) for financial support within the Collaborative Research Center SFB 1153, in particular subproject B02. (DFG Project number 252662854).

References

[1] B.-A. Behrens, J. Uhe, I. Ross, J. Peddinghaus, J. Ursinus, T. Matthias, S. Bährisch, Tailored Forming of hybrid bulk metal components, International Journal of Material Forming, 15 (2022). https://doi.org/10.1007/s12289-022-01681-9.

[2] S. E. Thürer, A. Chugreeva, N. Heimes, J. Uhe, B.-A. Behrens, Process chain for the manufacture of hybrid bearing bushings, Production Engineering, 15 (2021). https://doi.org/10.1007/s11740-021-01028-4.

[3] A. Piwek, E. Ortlieb, C.-V. Ince, J. Peddinghaus, H. Wester, J. Uhe, A. Raatz, K. Brunotte, Analysis of Temperature and Stress Distribution on the Bond Properties of Hybrid Tailored Formed Components, Adv. Eng. Mater. 27 (2025) 2402031. https://doi.org/10.1002/adem.202402031.

[4] A. Piwek, J. Peddinghaus, J. Uhe, K. Brunotte, Influence of enlarged joining zone interfaces on the bond properties of tailored formed hybrid components made of 20MnCr5 steel and EN AW-6082 aluminium, Materials Research Proceedings 41 (2024) 792–801. https://doi.org/10.21741/9781644903131-87.

[5] A. Piwek, J. Peddinghaus, J. Uhe, K. Brunotte, Investigation of the joining zone formation of impact extruded hybrid components by varied forming sequence and partial cooling, Materials Research Proceedings 28 (2023) 591–600. https://doi.org/10.21741/9781644902479-64.

[6] A. Piwek, J. Peddinghaus, J. Uhe, K. Brunotte, Influencing the mechanical properties of pre-joined hybrid semi-finished products by impact extrusion, METAL 2023, Brno (2023). https://doi.org/10.37904/metal.2023.4633.

[7] C.-V. Ince, A. Chugreeva, A. Böhm, A design concept of active cooling for tailored forming workpieces during induction heating, Production Engineering, 15 (2021) 177–186. https://doi.org/10.1007/s11740-021-01027-5.

[8] B.-A. Behrens, J. Uhe, T. Petersen, C. Klose, S. E. Thürer, J. Diefenbach, A. Chugreeva, Challenges in the Forging of Steel-Aluminum Bearing Bushings, Materials, 14 (2021) 803. https://doi.org/10.3390/ma14040803.

[9] B.-A. Behrens, J. Uhe, et al., Tailored Forming of Hybrid Bevel Gears with Integrated Heat Treatment, Procedia Manufacturing, 2020 (ScienceDirect article: S2351978920313007).

[10] F. P. Incropera, D. P. DeWitt, T. L. Bergman, A. S. Lavine, Fundamentals of Heat and Mass Transfer, 7th ed., Wiley, Hoboken, 2011.

[11] V. Rudnev, D. Loveless, R. L. Cook, Handbook of Induction Heating, 2nd ed., CRC Press, Boca Raton, 2017.

[12] G. Liang, I. Mudawar, Review of spray cooling – Part 1: Single-phase and nucleate boiling regimes, and critical heat flux, International Journal of Heat and Mass Transfer, 115 (2017) 1174–1205. https://doi.org/10.1016/j.ijheatmasstransfer.2017.06.029.

[13] G. Liang, I. Mudawar, Review of spray cooling – Part 2: High temperature boiling regimes and quenching applications, International Journal of Heat and Mass Transfer, 115 (2017) 1206–1223. https://doi.org/10.1016/j.ijheatmasstransfer.2017.06.022.

[14] J. Wendelstorf, K.-H. Spitzer, R. Wendelstorf, Spray water cooling heat transfer at high temperatures and liquid mass fluxes, International Journal of Heat and Mass Transfer, 51 (2008) 4902–4910. https://doi.org/10.1016/j.ijheatmasstransfer.2008.01.032.

[15] I. Vladyko, A. Kvochka, M. Raudensky, Analysis of the Influence of Nozzle-to-Surface Distance on the Cooling Process Characteristics, Fluids, 8 (2023) 191. https://doi.org/10.3390/fluids8070191.

[16] B.-A. Behrens, A. Chugreeva, J. Diefenbach, C. Kahra, S. E. Thürer, J. Uhe, Microstructural characterization of steel–aluminum hybrid components manufactured by friction welding and die forging, Metals, 10 (2020) 1365. https://doi.org/10.3390/met10101365.

[17] I. M. Sobol', Global sensitivity indices for nonlinear mathematical models and their Monte Carlo estimates, Mathematics and Computers in Simulation, 55 (2001) 271–280. https://doi.org/10.1016/S0378-4754(00)00270-6.

[18] H. Amend, Einfluss variabler Prozessparameter auf das Erzeugen axialer Temperaturgradienten in hybriden Bauteilen, Master Thesis, Leibniz University Hannover, 2025.

[19] D. C. Montgomery, Design and Analysis of Experiments, 8th ed., Wiley, Hoboken, 2013.

[20] J. Benther, et al., Heat transfer during multiple droplet impingement and spray cooling: Review and prospects for enhanced surfaces, International Journal of Heat and Mass Transfer, 178 (2021) 121587.

[21] M. Chabicovsky, P. Kotrbacek, H. Bellerova, J. Kominek, M. Raudensky, Spray Cooling Heat Transfer above Leidenfrost Temperature, Metals, 10 (2020) 1270. https://doi.org/10.3390/met10091270.

[22] H. Ghari, et al., Metallurgical characteristics of aluminum–steel joints manufactured by rotary friction welding: A review and statistical analysis, Journal of Materials Research and Technology, 2024 (ScienceDirect article: S2238785424006185).

The publication of this article was funded by the Leibniz Universität Hannover (LUH) / Technische Informationsbibliothek (TIB)